Eur Biophys J (2011) 40:795–804
DOI 10.1007/s00249-011-0695-2

ORIGINAL PAPER

Grading of intrinsic and acquired cisplatin-resistant human melanoma cell lines: an infrared ATR study

A. Zwielly · S. Mordechai · G. Brkic · E. Bogomolny · I. Z. Pelly · R. Moreh · J. Gopas

Received: 25 December 2010 / Revised: 13 March 2011 / Accepted: 16 March 2011 / Published online: 7 April 2011
© European Biophysical Societies' Association 2011

Abstract Attenuated total reflection (ATR) spectroscopy is used as an in vitro optical approach for the diagnosis and characterization of cell and tissue pathology. In comparison with the more conventional FTIR microspectroscopy that relies on transmission of IR radiation, ATR spectroscopy uses the evanescent wave technique, which is a step forward toward in vivo research. The aim of the present investigation was to examine the potential of ATR spectroscopy to differentiate between drug-resistant and drug-sensitive melanoma cell lines. We studied two human melanoma parental cell lines, GA and BG, and their cisplatin-resistant counterparts, GAC and BGC, respectively, which were derived by survival selection with this anticancer drug. Cisplatin cytotoxicity was measured on the four cell lines, and their relative resistance to cisplatin was established: BGC > BG > GAC > GA. Different resistance mechanisms were noticed between the two parental groups in accordance with their spectrum. ATR spectra-based cluster analysis of the selective biomarkers, such as phosphate and RNA/DNA, were found useful in differentiating sensitive from resistant cells. Normalized and absolute values of the differences between spectra were employed to compare between the two parental groups. It was possible to predict the relative cisplatin resistance between the cell lines using the discriminant classifying function. The success rates in predicting cisplatin resistance in these cells was 88 and 81% for GA versus GAC and BG versus BGC, respectively. These results support the further development of the ATR technique as a simple, in vitro, reagent-free method to identify drug resistance in cancer cells.

Keywords Malignant melanoma · Attenuated total reflection (ATR) · Discriminant classifying function (DCF) · Cisplatin · Drug resistance

A. Zwielly · S. Mordechai (✉) · E. Bogomolny · R. Moreh
Department of Physics and the Cancer Research Center, Ben-Gurion University, Beer-Sheva 84105, Israel
e-mail: shaulm@bgu.ac.il

G. Brkic · J. Gopas
Department of Microbiology and Immunology, Faculty of Health Sciences, Ben Gurion University, Beer-Sheva, Israel

I. Z. Pelly
Department of Geological and Environmental Sciences, Faculty of Natural Sciences, Ben Gurion University, Beer-Sheva, Israel

J. Gopas
Department of Oncology, Soroka University Medical Center, Beer-Sheva, Israel

Introduction

Acquired drug resistance is a common occurrence in many diseases and is considered as the main reason for malignant cancer treatment failure. The phenomenon takes place when tumor cells are selected by chemotherapy treatment, remain in the patient and eventually show up as a drug-resistant tumor that will no longer respond to treatment with that or other drugs (multidrug resistance). Of more than 500,000 annual deaths from cancer in the United States, many are a result of the development of resistance to chemotherapy. Drug resistance has been described as "the single most common reason for discontinuation of a drug" (Zamble and Lippard 1995). The emergence of resistance depends in part on the genetic instability, heterogeneity and high mutational rate of tumor cells (Melnikova and Bar-Eli 2008; Brkic et al. 2003).

Melanoma is a malignant tumor of melanocytes that are found predominantly in skin. It is one of the rarer types of skin cancer but causes the majority of skin cancer-related deaths. The basis for drug resistance in melanoma is most likely deregulation of apoptosis, although other mechanisms, including drug transport, detoxification and enhanced DNA repair, may also play a role (Tawbi and Buch 2010).

Determination of the chemotherapeutic drug of choice with the highest probability of success and monitoring the emergence of drug-resistant tumor cells after treatment are a challenging mission. This is especially true in melanoma were various chemotherapy agents are used to treat metastatic melanoma, but the overall success is quite limited, since this tumor type is usually intrinsically resistant to anti-cancer drugs.

Cell cultures have been the focus of many drug resistance-related investigations. The uniqueness of cell lines allows the rapid accumulation of mutation and their selection, which can be generated in days, while tissues that will become resistant usually undergo a series of dysplastic changes over a time span of many months or even years (Bogomolny et al. 2009, 2010; Sule-Suso et al. 2004). In addition, cell cultures are advantageous as compared to primary tissues because of their immortality and homogeneity, and the ability to control and monitor important culture parameters, such as growth and drug resistance. Moreover, morphological changes can be monitored by microscopic techniques in parallel with the spectral measurements. Thus, cell cultures provide an ideal model for detecting cellular spectral changes during malignant cell progression that can be extended and further validated in vivo.

IR spectroscopy has shown encouraging trends in the field of cancer diagnosis in the last 20 years (Lasch et al. 2004; German et al. 2006; Yang et al. 2005; Bird et al. 2009; Miller et al. 2010). One of the crucial issues with matter-light interaction is that cell lines and other biological systems contain essential water amounts. Water solutions are totally opaque to IR radiation; therefore, it is generally convenient to carry out measurements on such systems using an attenuated total reflectance (ATR) crystal. ATR enables measuring spectra in aqueous solutions (Wang 2006). An IR beam that passes through the ATR crystal in contact with the sample forms the evanescent wave. The radiation typically extends into the sample by a few micrometers. The penetration depths as well as the unique interaction of the radiation with the sample (Urban 1996) form an IR spectrum with unique features. The need for rapid and portable in vivo diagnostic instrumentation places the ATR platforms in the forefront of diagnostic research. Most promising among the many evanescent wave instruments are fiber optics and portable ATR-based probes (Hammody et al. 2007). These real-time, rapid diagnosis modalities include the possibility to detect and define drug-resistant versus drug-sensitive tumors as well as their degree of resistance to a specific drug.

Platinum-based drugs are widely used in the treatment of cancer. They form intra-strand and inter-strand Pt-DNA cross-links, which kill the cell if inadequately repaired. Two DNA repair systems are predominantly involved in coping with Pt-DNA adducts: Nucleotide excision repair (NER) is required for adduct excision and homology-directed DNA repair (HR), which is required for precise repair of the DNA breaks remaining after adduct removal. Cisplatin is one of the most common drugs used for melanoma treatment (Kelland 2007). Even though cisplatin has proven to be a highly effective chemotherapeutic agent for treating various types of cancers, it has encountered the same fate as many other drugs used in cancer chemotherapy, namely, drug resistance. When cells become resistant to cisplatin, the doses must be increased, but a large-dose escalation can lead to severe multiorgan toxicities, especially in kidneys and bone marrow.

Previous works show the potential of IR spectroscopy for early identification of drug resistance (Draux et al. 2009). We have successfully investigated the ability of FTIR microscopy to define spectral changes between drug-sensitive and drug-resistant human melanoma cell lines (Zwielly et al. 2009). In this research, we expand our findings to another parental and drug-resistant human melanoma cell line pair. In contrast to our previous work, here we use the ATR technique to compare the spectra between sensitive and resistant cells of two pairs of parental and cisplatin-resistant cell lines in a controlled experimental set up that is one step forward toward future in vivo measurements.

Identifying resistance of human melanoma cells to specific drugs using a simple, in vitro, reagent-free method such as ATR can contribute in the future to the rapid detection of drug-resistant tumors in patients. In addition, successful results will stimulate the development of more advanced portable ATR-based instruments as well as appropriate classifying algorithms for detection. Eventually, the successful application of this technique will contribute to the ability of the physician to choose an effective treatment protocol to the individual patient.

Materials and methods

Cell lines

GA and BG parental cell lines (Fig. 1) were established from metastatic explants of two different melanoma patients (Brkic et al. 2003). The cells were maintained in DMEM medium supplemented with 5% L-glutamine,

5% antibiotics (streptomycin and penicillin) and 10% fetal calf serum (Biological Industries, Kibbutz Beit Haemek, Israel) and regularly propagated by trypsinization. Cells were grown on glass slides and stained with a standard hematoxylin-eosin protocol.

GA and BG cisplatin-resistant cell lines (GAC and BGC, respectively) were obtained by a single-step selection protocol, as reported earlier (Brkic et al. 2003). Briefly: 10^6 of each cell was treated with the LD_{90} concentration of cisplatin for 5 days. The cells were washed with PBS and allowed to propagate and stabilize in fresh medium. The drug-selected cells were isolated and tested for resistance to cisplatin by determining the LD_{50} cytotoxic concentration of cisplatin. Cell viability was determined by the neutral red assay (Jonston et al. 1981). The LD_{50} of GAC cells after 48 h incubation with the drug was 65 μM, as compared to 20 μM, the LD_{50} of GA cells. Thus, GAC cells are 3.25 more resistant to cisplatin than the parental GA cells. For BGC cells, the LD_{50} cytotoxic concentration was 140 μM as compared to 85 μM for BG cells. Thus, BGC cells are 1.65 more resistant to cisplatin than BG cells (Tanic et al. 2006). Although morphological differences between GA and BG cells can be seen in Fig. 1, no significant morphological differences were observed between the parental cells and their respective cisplatin-resistant counterparts (not shown).

Sample preparation for ATR measurements

Cell cultures were washed with a physiological saline solution and harvested from the tissue culture plates after treatment with trypsin (0.25%) for 2 min. The cells were washed three times with saline by centrifugation at 1,000 rpm for 7 min then resuspended at a concentration of 10^6 cells/ml. The number of cells was counted with a hematocytometer. Four drops each of 1 μl (1,000 cells/μl) were placed on the zinc sellenide crystal to cover it entirely and then dried for 1 h with an air flow. The dried cell smears typically produced monolayer cells of about 10 μm thickness (Zwielly et al. 2009).

Attenuated total reflectance spectroscopy and data acquisition

This technique is based on the phenomenon of attenuated total reflection. Our system is composed of a modified FTIR spectrometer (Bruker, Tensor Vector 27; Karlsruhe, Germany). The spectrometer is equipped with a liquid nitrogen cooled mercury-cadmium-telluride (MCT) detector and coupled with a Horizontal Attenuated Total Reflectance Accessory (Fig. 2). The horizontal Attenuated Total Reflectance Accessory is connected with a nitrogen reservoir, which enables preserving the dryness of the sample. The compact design of the accessory employs a pair of transfer optics to direct the infrared beam to one end of the IR transmitting crystal (Fig. 2).

The penetration depth (d_p) of the evanescent IR radiation into the sample can be calculated using the relation from Maxwell equations (Harrick 1979)

$$d_p = \frac{\lambda / n_c}{2\pi\sqrt{\sin^2 \alpha - n_{sc}^2}} \quad (1)$$

where n_c is the refractive index of the crystal, n_{sc} is the ratio of the refractive indices of the sample and the ATR crystal, and α is the angle of incidence as can be seen in the magnified region in Fig. 2 (based on HATR, PIKE Technologies Inc. scheme).

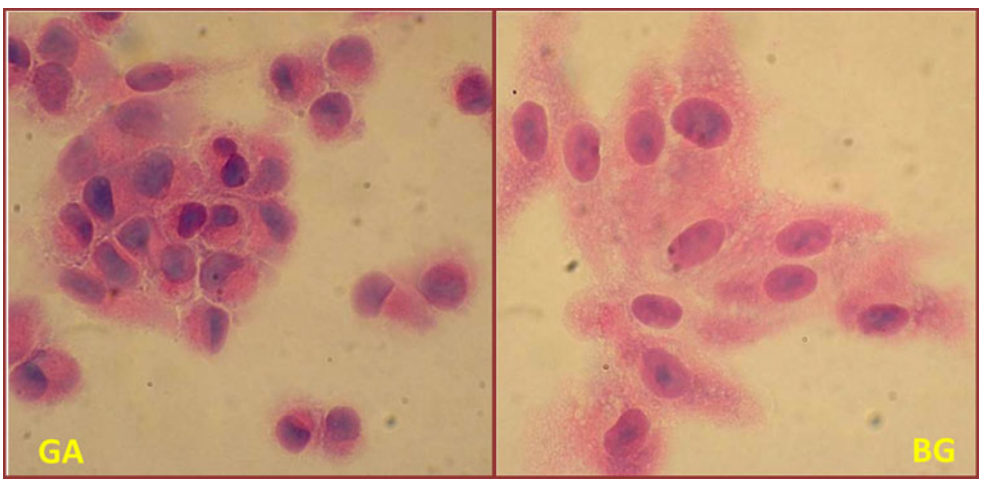

Fig. 1 GA and BG melanoma cells were grown on glass slides as described in "Materials and methods." When the cells reached 50% confluence, they were stained with hematoxylin-eosin. GAC and BGC cells were morphologically undistinguishable from their corresponding parental cells; therefore, they are not presented in here. Magnification: ×600

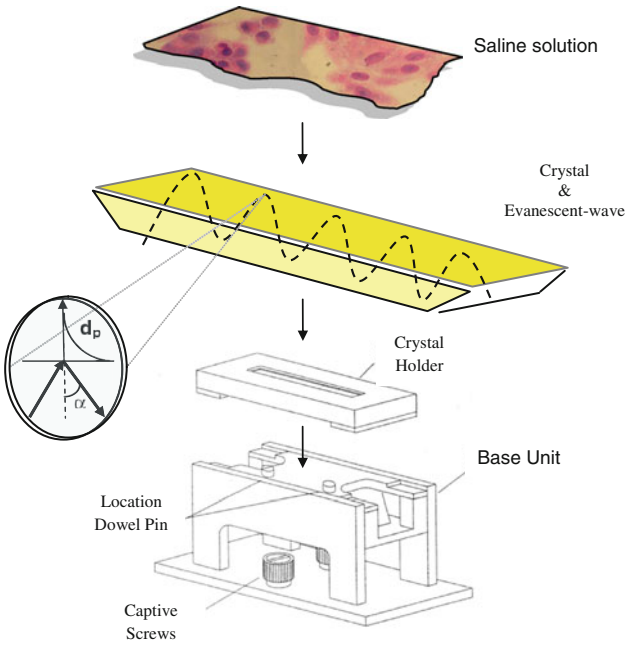

Fig. 2 ATR Schematic Setup (*top–bottom*): The cell line sample was spread and dried on the trapezoidal ZnSe crystal with a refractive index of 2.4 at 1,000 cm^{-1} and incidence angle of 45° (magnified region). The crystal was placed on the holder over the base unit. The IR waves transmit trough the crystal and sample the deposit cell layer

To achieve a high signal-to-noise ratio (SNR), 128 co-added scans were collected in each measurement in the wave number region of 600–4,000 cm^{-1}. Baseline correction and normalization were performed for all the spectra using the rubber band method in OPUS software. For the construction of the baseline, each spectrum was divided up into 64 segments of equal size. In each spectral range, the minimum y-value was determined. The baseline was then created by connecting the minima with straight polynomial lines. Starting from "below," a rubber band stretched over this curve constituted the baseline.

Statistical analysis

The obtained parameters (biomarkers) were classified using cluster analysis according to Ward's method (Everitt 1980) and the discriminant classification function (DCF) method (Huberty 1994; Fisher 1936). DCF is a statistical tool that enables improving classification between gradually evolved subgroups simultaneously using several spectral variants. DCF generates a classification score for each group that is a linear combination of a previously derived array of biomarkers with weight coefficients given by the following equation:

$$S = c + w_1 \cdot \boldsymbol{x_1} + w_2 \cdot \boldsymbol{x_2} + \cdots + w_m \cdot \boldsymbol{x_m} + \cdots \quad (2)$$

where w_m is the weight coefficient, x_m is the biomarker value, and S denotes the resultant classification score. In previous works we employed the DCF based on the *t*-test values to classify the normal polyps and malignant tissues into separate groups (Zwielly et al. 2010). The *t*-test values were considered significant at $P < 0.05$.

Results

The aim of this work was to test the potential of ATR spectroscopy to identify the major differences between resistant and sensitive human melanoma cells and to validate this optical methodology in tandem with advanced statistical techniques for identifying drug resistance. Two different cell line pairs and their cisplatin-resistant variants (C) have been studied: GA/GAC and BG/BGC, a total of four different cell lines. The spectrum of each cell line was determined separately and was analyzed in the context of its sensitivity to cisplatin, as determined by a cytotoxic test. The morphology of the parental GA and BG cell lines is presented in Fig. 1. Both GA and BG are adherent cells. When grown in vitro, the cells lose melanin expression, but regain the ability to synthesize melanin when grown in athymic mice. GA cells are more rounded and less adherent than BG since they can be detached faster with trypsin. BG cells have a more elongated morphology, more granular cytoplasm and prominent (one or two) nucleoli than GA. No significant morphological differences were observed between the parental cells and their respective cisplatin-resistant counterparts (not shown).

The uniqueness of the ATR approach is that the cells are sampled with the evanescent field where the light intensity decays exponentially as a function of the distance from the reflecting interface. In turn, the spectral differences may arise from either a difference in the chemical composition or from a different distribution of the biochemicals along an axis perpendicular to the reflecting interface. This feature precludes definitive conclusions on the overall chemical composition of the different cell lines.

Biochemical spectra interpretation

Figure 3 shows the full range mean spectra: 800–4,000 cm^{-1} of (a) the BG versus BGC (b) GA versus GAC cells. The difference spectrum between these two groups with its standard deviation is shown (c) BG minus BGC (d) GA minus GAC. The wave numbers listed in Fig. 3c, d represent significant biomarkers. The highlighted gray areas in Fig. 3a, b emphasize regions with reverse trends between the two main groups GA and GAC, and BG and BGC cells. These regions determine that a different resistance mechanism to cisplatin is active in each one of the cells pairs. The intense water symmetric stretch absorption is included in the region of 3,000–4,000 cm^{-1} that masks other useful

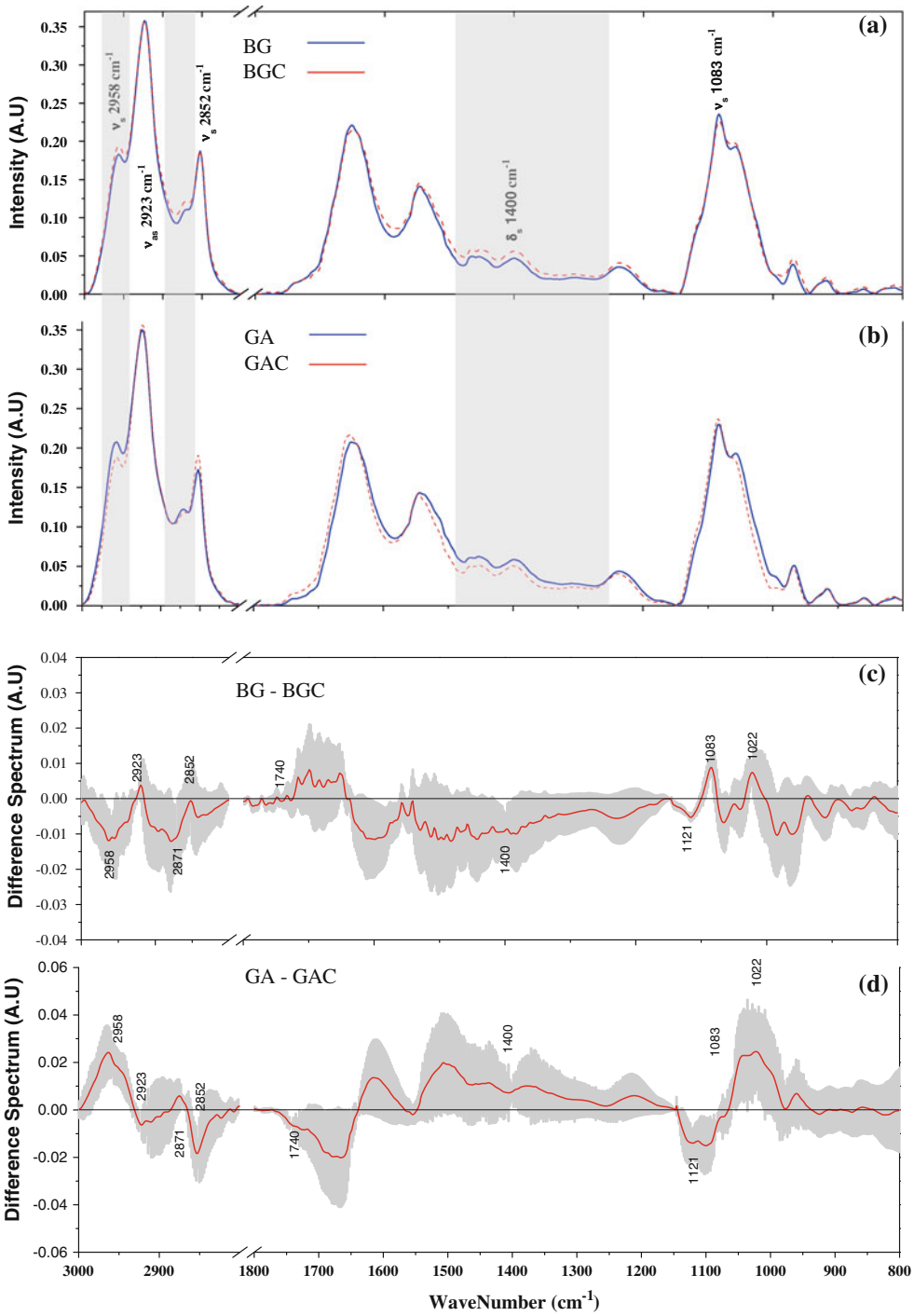

Fig. 3 Mean of all ATR recorded spectra in the measured 800–3,000 cm^{-1} wave number range **a** BG versus BGC, **b** GA versus GAC. The difference spectra with their standard deviations **c** BG-BGC, **d** GA-GAC are shown

vibration bands. In contrast to the case of transmittance FTIR microscopy (Sahu et al. 2005) where the IR radiation interacts with a sample that has been seeded on a zinc selenium glass and dried in a fume-chamber control surround, the ATR approach is different. The in vivo nature of the ATR technique required us to seed the harvested cells directly on the zinc-selenium crystal and dry them in real-time. For this reason the embedded water in the sample is less controlled, and the measured spectra will change with time because of the decreasing water content. It is important to measure for a long time until the water has vaporized and the influence is inconspicuous. The 2,800–3,000 cm^{-1} region after background subtraction is less sensitive to the water content and contains important information about the methyl and methylene groups in the cells. This region shows remarkable changes in the case of GA/GAC (Fig. 3a), while slight changes are apparent in the BG/BGC cells (Fig. 3b). The intensity ratio A(2,958)/

A(2,852) or ν_{as} CH_3/ν_s CH_2 is significant between the GA versus GAC cells, while showing almost no difference in the BG versus BGC cells (Table 1). This ratio is composed of the 2,852 cm^{-1} band and the 2,923 cm^{-1} band, which originate from the symmetric/antisymmetric stretching of the methylene chains in membrane lipids, respectively. The second member in this ratio is the 2,958 cm^{-1} and the 2,871 cm^{-1} bands arising from the antisymmetric/symmetric CH_3 (methyl) stretching, respectively.

The 1,800–2,800 cm^{-1} region is completely uninformative, containing mainly the vibration modes of the surrounding cells' CO_2 affixture. This region shows a clear convex curve shape in all four cell spectra.

The 1,400–1,800 cm^{-1} region is almost solely subjugated to the conformation-sensitive amide I and amide II bands, which are the most dominant bands in the spectra of nearly all complex biological systems (Gremlich and Yang 2001). The intensity differences over the amide I integrated absorbance are significant in both groups and show reverse trends between them (Table 1). Amide I is among the bands that slightly shift between the various groups. In particular, the amide I in the GA spectra appears at lower wave numbers and wider with respect to the GAC spectra (data not show). Since amide I arises from the C=O hydrogen bonded stretching vibrations (Diem et al. 2008), these changes may arise because of biochemical alterations (conformation and composition) in protein and/or nucleic acids, respectively. The amide I band comprises several major absorption bands, such as $\sim$1,654 cm^{-1}, which corresponds to the secondary structure of proteins, specifically, increases for GAC compared to GA, while no significant change is noticed between the BG and BGC cells. The 1,639 and 1,627 cm^{-1}, due to alpha helix, random coil and parallel beta strand structures, respectively, show a slight decrease for the GAC over the GA, but again no similar changes are observed for the BG and BGC groups.

The A(1,740)/A(1,400) ratio was found to be a promising biomarker in our previous research with FTIR microspectroscopy on GA/GAC cells (Zwielly et al. 2009). In agreement with our previous study, a significant increase is noticed for the GA cells compared to GAC cells. A smaller but yet significant decrease is noticed for the BGC over the BG cells.

The 1,083 cm^{-1} band (ν_s PO_2^- of phosphodiesters of nucleic acid) shows no changes for the GA/GAC cells and a decrease for the BGC over the BG cells. The reverse trend appears for the 1,056 cm^{-1} (O–H stretching coupled with C–O bending of C–OH groups of carbohydrates) where the BG/BGCs have the same absorbance, while the GAC decreases compared to the GA cells. An increase in DNA absorbance at 966 cm^{-1} (due to C–C/C–O stretching of deoxyribose-ribose vibration) and at 780 cm^{-1} (sugar-phosphate vibrations) is noticed for the resistive type of BGC cells compared to the BG cells. The GA/GAC groups show a slight decrease for the 966 cm^{-1} and the same value for the 780 cm^{-1} band (Table 1).

Cluster analysis

Cluster analysis was used to discriminate between cells within each of the two groups: GA versus GAC and BG versus BGC cells. Using a test-failure approach, we applied the cluster analysis algorithm to the significant wave numbers (Fig. 3c, d) in order to achieve the best separation results. Six of the significant wave numbers from the spectra—1,022, 1,121, 1,400, 1,740, 2,852 and 2,958 cm^{-1}—were chosen for the GA/GAC group. The derived three ratios A(1,121)/A(1,022), A(2,958)/A(2,852) and A(1,740)/A(1,400), were found to yield better separation results for the GA/GAC group. In the case of the BG/BGC group, the A(1,121)/A(1,022) ratio and the 2,958, and 1,400 cm^{-1} wave numbers were applied. Using our large number of measurements, the results of the complete tree look crowded if all data points are present in the dendrogram. By consolidating lower branches of the tree, the dendrogram's initial branches represent several measurements together as necessary.

The results presented in Fig. 4 show that cluster analysis can indeed discriminate the sensitive cells from the resistant type for both groups of cells. The following terminology was used to estimate the prediction rates:

$$\text{Success rate} = \frac{\mathrm{N}_{\text{true\_positive}} + N_{\text{true\_negative}}}{N} \times 100 \quad (3)$$

$$\text{False negative rate} = \frac{N_{\text{false\_negative}}}{N_{\text{positive}}} \times 100 \quad (4)$$

N is the total number of measurements, $N_{\text{true\_positive}}$ is the number of true positives in each group, $N_{\text{true\_negative}}$ is the number of true negatives in each group, $N_{\text{false\_negative}}$ is the number of false negatives in each group, and N_{positive} is the number of positive cases in each group.

The GA/GAC cells can be classified with an average 88% success rate (Fig. 4a), while in the case of BG/BGC cells an 81% success rate was achieved (Fig. 4b). The results are summarized in Table 2. We note that in both cases, morphological distinction within each group is impossible.

Grading and classification of drug-resistance using the DCF statistical tool

Figure 5a shows the cytotoxic test for the four groups: GA, GAC, BG and BGC. The LD50 of cells after 48 h incubation with the drug was as follow: GAC 65 μM, as compared to 20 μM for GA cells, whereas BGC LD50 is

Table 1 Important biomarkers: average absorbance intensities and standard deviations

WN (cm^{-1})	Type				
	GA	GAC	BG	BGC	Interpretation
2,958	0.206 ± 0.004	0.185 ± 0.003	0.189 ± 0.004	0.192 ± 0.002	ν (CH_3) asymmetric
2,923	0.350 ± 0.0004	0.353 ± 0.0004	0.357 ± 0.0003	0.355 ± 0.0005	ν (CH_2) asymmetric
2,871	0.123 ± 0.0013	0.112 ± 0.0007	0.115 ± 0.0008	0.122 ± 0.0005	ν (CH_2) symmetric
2,852	0.173 ± 0.005	0.190 ± 0.001	0.187 ± 0.0009	0.188 ± 0.005	ν-(CH_3) symmetric
1,740	0.008 ± 0.0003	0.015 ± 0.0002	0.014 ± 0.0003	0.014 ± 0.0006	ν (C=O) of esters
1,650	0.207 ± 0.0015	0.216 ± 0.0006	0.217 ± 0.0007	0.214 ± 0.0006	ν (C=O) amide I; α-helix
1,639	0.203 ± 0.0007	0.203 ± 0.0004	0.206 ± 0.0003	0.207 ± 0.0004	β-pleated sheet (Amid I)
1,630–1,700	10.174 ± 0.1	11.036 ± 0.05	10.868 ± 0.048	10.813 ± 0.05	Amid I-integration area
1,400	0.058 ± 0.0001	0.051 ± 0.0001	0.049 ± 0.0006	0.056 ± 0.0008	ν (C=O) symmetric- proteins
1,121/1,022	0.89 ± 0.036	1.7 ± 0.085	1.08 ± 0.035	1.16 ± 0.045	RNA/DNA Ratio
1,083	0.230 ± 0.0002	0.235 ± 0.0002	0.233 ± 0.0001	0.225 ± 0.0002	ν (CN) Carbohydrates
1,056	0.192 ± 0.001	0.182 ± 0.0005	0.191 ± 0.0009	0.180 ± 0.001	ν (P=O) symmetric of PO_2^-

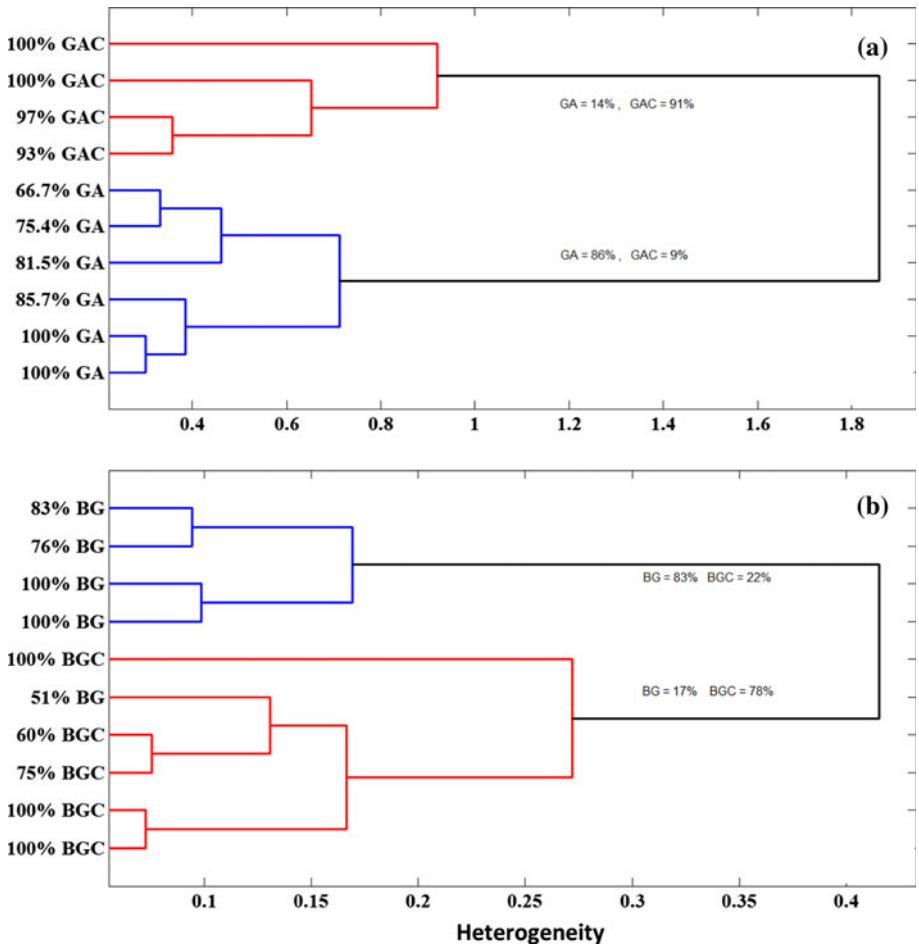

Fig. 4 Cluster analysis dendrogram based on six selective wave numbers extracted from the IR spectra of (**a**) GA versus GAC (**b**) BG versus BGC cell lines

140 μM, as compared to 85 μM for BG cells. Thus, GAC cells are 3.25 more resistant to cisplatin than GA cells, and BGCs are only 1.65 more resistant to cisplatin than BGs.

GA, GAC and BG, and BGC cells constitute two genetically independent groups; therefore, it is of interest to detect a possible digital grading of the cells based only on a chosen set of biomarkers. Based on these biomarkers, the resistance level could be calculated, and the groups can be classified regardless of their source.

Table 2 Cluster analysis: successful and false-negative identification percentages

	GA	GAC	BG	BGC
Success rate	91%	86%	83%	78%
False-negative	9%	14%	17%	22%
Number of measurements	42		36	

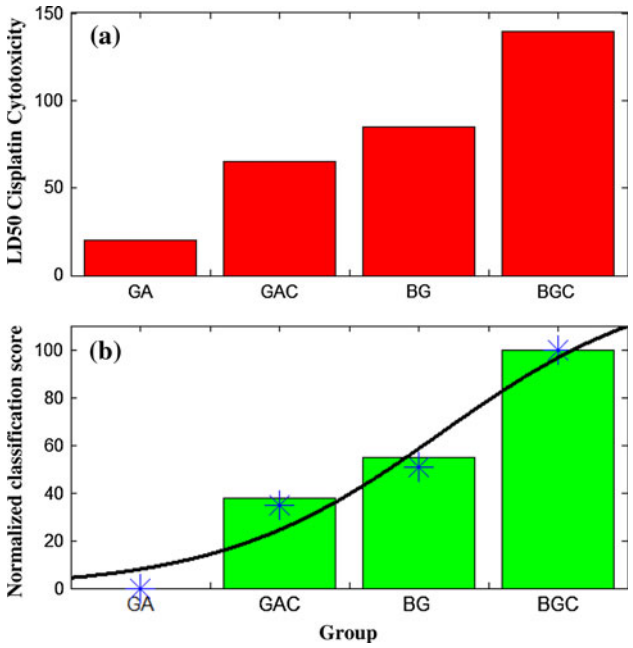

Fig. 5 **a** LD_{50} neutral red cisplatin cytotoxic test results for each of the cell lines. **b** Discriminant classification function (DCF) of GA, GAC, BG and BGC cells. Each class is represented by an array of average values of four biomarkers. The *green bars* represent the normalized cytotoxic test for each cell

The array of biomarkers that was found most suitable in predicting the resistance of each one of the cells was as follows:

$$\begin{pmatrix} A_{2871} \\ A_{2923} \\ A_{1400} \\ A_{1083} \end{pmatrix} \quad (5)$$

To further examine the gradual spectral changes encountered in the above cell samples, we utilized the discriminant classification function (DCF). This statistical tool enables improving discrimination between GA, GAC, BG and BGC cells by representing an adequate quantitative follow-up of transformations versus group type. DCF generates a classification score for each cell type or drug-resistant stage using a linear combination of a previously derived array of biomarkers with weight coefficients (Huberty 1994). In our case the coefficients are based on the significant respective t test values. Figure 5b shows the absolute score values of each group based on Eq. 2. The red bars represent the 48-h cytotoxic results for each individual cell type.

It is noticed, as expected, that the BG and BGC cells have similar scores, which means that only small detectable spectral changes occur between BG and BGC cells compared to the GA/GAC cells. Generally, the score values of the cells starting with the GA cells gradually approach the spectral values of the highest resistance BGC group as indicated from the cytotoxic test (Fig. 5).

Discussion

ATR spectroscopy was used to examine the differences between cisplatin resistance and sensitivity patterns of two independent human melanoma cell lines.

By comparing the full range spectrum between GA/GAC and BG/BGC pairs, we detected regions that are intrinsic for each cell type (GA vs. BG) as well as opposite in spectral signature between the pairs (GA/GAC vs. BG/BGC) (Fig. 3). One of the bands showing this trend is the 1,300–1,500 cm^{-1} spectral region. It is comprised primarily of vibration modes arising from amino acid residues as well as stretching and bending modes of the membrane lipids. The first broad prominent feature in this region centered at 1,456 cm^{-1} contains overlapping bands at δ 1,464 cm^{-1}, δ 1,456 cm^{-1} (due to CH_2 in lipids) and δ_{as} 1,446 cm^{-1} (due to CH_3 in lipids), while the second prominent band at 1,400 cm^{-1} represents the ν_s C=O in proteins (Parker 1971). The other two highlighted regions in Fig. 3 include the vibrational modes ν_{as} CH_2 at 2,923 cm^{-1} and ν_s CH_2 at 2,852 cm^{-1} that together with the ν CO at 1,056 cm^{-1} (not included in this region) correspond to lipid bands. These changes were most prominent compared to other bands, since the evanescent waves do not penetrate the internal cellular structures and organelles, and therefore the masking effect of other bands on the lipids absorbance is minimal.

The spectral differences between the GA/GAC and the BG/BGC suggest the occurrence of fundamentally different mechanisms of cisplatin resistance between the two groups. These results are not surprising since a wide range of resistance mechanisms to cisplatin have been identified in cancer cells. They fall into three main categories: (1) decreased accumulation of cisplatin in resistant cells; (2) increased intra-cellular trapping of cisplatin; (3) increased repair of DNA damage or increased tolerance of DNA damage (Kelland 2007).

Indeed, it seems that BG and GA parental cell lines express significant and intrinsic differences in cisplatin-resistance mechanisms. We have demonstrated (unpublished

data) that GA cells accumulate cisplatin twice faster than BG; they express half the amount of glutathione (GSH) and are more sensitive to cisplatin-induced apoptosis and DNA fragmentation.

Using cluster analysis, we differentiated between the cell lines within each group. It is not surprising that the GA/GAC pair was better differentiated than the BG/BGC pair, because the cisplatin sensitivity ratio between GA/GAC cells is approximately two-fold higher than the ratio between BG/BGC cells (Fig. 5a). It is also noticed that the distance between the GA and GAC clusters is 1.8 (Fig. 4a) relative to 0.42 in the BG/BGC case (Fig. 4b). This is in agreement with the cisplatin cytotoxic test results (Fig. 5a). Another marker of importance that enables better differentiation of the GA/GAC pair is the ordered appearance of classified members, i.e., 100% GAC in the top node toward 100% GA in the lower node. In contrast, the BG/BGC group shows a mixed pattern between BG and BGC (Fig. 5b).

Using the absolute values of the differences between the cells, we succeeded in grading the resistance type of all four members in this study based on selective biomarkers (Fig. 5b).

The BG highly intrinsic resistance to cisplatin combined with its closeness to BGC cells can result in ATR signal saturation. This means that the built-in resolution limitation of the ATR will result in a restricted ability to discriminate between these two cell lines as compared to the GA/GAC pair.

We have previously compared the GA/GAC cells by FTIR-MSP (Zwielly et al. 2009) in which a small number of cells was studied in each sample. By contrast, a large number of cells are used in each of the ATR measurements, resulting in data that are more statistically significant. In addition, evanescent wave absorbance techniques such as ATR, rather than microscopic transmission radiation techniques such as FTIR-MSP, enable possible in situ/in vivo implementation. An in-depth comparison between these two techniques requires a separate discussion.

Studying drug impact on Calu-1 cancer cells using IR spectroscopy was also done by Draux et al. (2009). In their study, FTIR spectroscopy was employed on cells of lung cancer in order to identify early cellular events in response to gemcitabine, an anti-tumor drug. Their conclusion was in agreement with our results showing that subtle spectral information can be acquired from cells treated with chemotherapeutic drugs. Similarly to our study, cluster analysis was employed that successfully classified the Calu-1 cell exposure to different drug doses.

In another study conducted by Baker et al. (2010), prostate cancer cell lines were successfully discriminated based on their IR and Raman spectra. Epithelial cells derived from the peripheral zone of the histopathologically normal adult prostate were transformed with a single copy of human papillomavirus 18 to establish the non-tumorigenic RWPE-1 cell line. These cells were further transformed to a total of five derivative groups. Using PCA analysis together with pseudo-3D discriminant functions, all six groups were classified with the highest sensitivity of 100% and lowest of 85%. These high separation rates are similar to the ranges in our classification.

Although our success rates in predicting cisplatin resistance were high, 88% and 81% for GA versus GAC and BG versus BGC, respectively, it is not yet high enough for a diagnostic procedure. A reliable discriminating test to be used in vivo requires higher sensitivity and specificity. Most likely, other parameters that cannot be measured accurately by the ATR method also play a role, such as methods that measure reduced transport of cisplatin across membranes or reduction of cisplatin-DNA adduct formation. To further refine our ability to discern between the cells, the ATR method should be optimized by developing more advanced ATR equipment with a better SNR and improved analysis techniques such as neural networks that demand larger databases. Ideally, ATR should be used in conjunction with other techniques or diagnostic parameters that may offer further differentiation between the cells such as DNA repair efficiency, multidrug transporter expression, BRAF mutations and the existence of cancer stem cells. In addition, more sensitive/resistant pairs of melanoma cell lines should be examined to identify and validate the significant biomarkers.

In conclusion, our studies together with studies of others show the potential of IR spectroscopy to detect biochemical changes in drug-resistant cancer cells. Our work extends to the ability to grade two different melanoma cell lines and their relative cisplatin resistance based on selective biomarkers extracted from the data and identified from the IR spectra. The benefit of ATR spectroscopy over other IR transmittance techniques is in its feasibility for in vivo diagnostic implementation as an ultimate goal.

Acknowledgments This work was supported by the Goldyne Savan Estate, the Richard H. Holzer Foundation and the Samuel Goldstein Memorial Foundation.

References

Baker MJ, Clarke C, Demoulin D, Nicholson JM, Lyng FM, Byrne HJ, Hart CA, Brown MD, Clarke NW, Gardner P (2010) An investigation of the RWPE prostate derived family of cell lines using FTIR spectroscopy. Analyst 135:887–894

Bird B, Bedrossian K, Laver N, Miljkovic M, Romeo M, Diem M (2009) Detection of breast micro-metastases in axillary lymph nodes by infrared micro-spectral imaging. Analyst 134:1067–1076

Bogomolny E, Mordechai S, Zwielly A, Huleihel M (2009) Early detection of premalignant changes in cell cultures using light-induced fluorescence spectroscopy. Eur Biophys J 38:971–980

Bogomolny E, Huleihel M, Salman A, Zwielly A, Moreh R, Mordechai S (2010) Attenuated total reflectance spectroscopy: a promising technique for early detection of premalignancy. Analyst 135(8):1934–1940

Brkic G, Gopas J, Tanic N, Dedovic-Tanik N, Benharroch D, Finkelstein-Jaworowsky E, Dimitrijevic B (2003) Identification of differentially expressed mRNA transcripts in drug-resistant versus parental human melanoma cell lines. Anticancer Res 23:2601–2607

Chu G (1994) Cellular responses to cisplatin. The roles of DNA-binding proteins and DNA repair. J Biol Chem 269:787–790

Diem M, Griffith P, Chalmers JM (2008) Vibrational spectroscopy for medical diagnosis. Wiley, p 40

Draux F, Jeannesson P, Gobinet C, Sule-Suso J, Pijanka J, Sandt C, Dumas P, Manfait M, Sockalingum GD (2009) IR spectroscopy reveals effect of non-cytotoxic doses of anti-tumour drug on cancer cells. Anal Bioanal Chem 395(7):2293–2301

Everitt B (1980) Cluster analysis. Wiley, New York

Fisher RA (1936) The use of multiple measures in taxonomic problems. Ann Eugenics 7:179–188

German M, Hammiche A, Ragavan N, Tobin MJ, Cooper JL, Matanhelia SS, Hindley AC, Nicholson CM, Fullwood NJ, Pollock HM, Martin FL (2006) Detection of colonic inflammation with Fourier transform infrared spectroscopy using a flexible silver halide fiber. Biophys J 90(10):3783–3795

Gremlich H, Yang B (2001) Infrared and Raman spectroscopy of biological materials. In: Dekker M (ed) NY, pp 421–475

Hammody Z, Huleihel M, Salman A, Argov S, Moreh R, Katzir A, Mordechai S (2007) Potential of 'flat' fiber evanescent wave spectroscopy to discriminate between normal and malignant cells in vitro. J Microsc 228(Pt 2):200–210

Harrick NJ (1979) Principles of internal reflection spectroscopy, chap. 2. In: Internal reflection spectroscopy, Harrick Scientific Corporation, Ossining, pp 13–66

Huberty C (1994) Applied discriminant analysis. Wiley, New York

Jonston MD, Fint ER, Young PA (1981) Dye uptake method for assay of interferon activity. Methods Enzymol 78:394–399

Kelland L (2007) The resurgence of platinum-based cancer chemotherapy. Nat Rev Cancer 7:573–584

Lasch P, Haensch W, Naumann D, Diem M (2004) Biochim Biophys Acta 1668:176–186

Marek W (1996) Urban attenuated total reflectance spectroscopy of polymers, theory and practice

Melnikova VO, Bar-Eli M (2008) Transcriptional control of the melanoma malignant phenotype. Cancer Biol Ther 7(7):997–1003

Miller M, Dumas P (2010) From structural to cellular mechanism with infrared microspectroscopy, current opinion in structural biology (20):1–8

Parker FS (1971) Application of infrared spectroscopy in biochemistry, biology and medicine. Plenum Press, NY, pp 477–491

Sahu RK, Argov S, Salman A, Zelig U, Huleihel M, Grossman N, Gopas J, Kapelushnik I, Mordechai S (2005) Can FTIR-spectroscopy at higher wavenumbers (mid IR) shed light on biomarkers for carcinogenesis in tissues. J Biomedical Optics 10:54017–54027

Sule-Suso J, Forster A, Zholobenko V, Stone N, El Haj A (2004) Effects of $CaCl_2$ and $MgCl_2$ on Fourier transform infrared spectra of lung cancer cells. Appl Spectrosc 58(1):61–67

Tanic N, Brkic G, Dimitrijevic B, Dedovic-Tanic N, Gefen N, Benharroch D, Gopas J (2006) Identification of differentially expressed mRNA transcripts in drug-resistant versus parental human melanoma cell lines. Anticancer Res 26(3A):2137–2142

Tawbi HA, Buch SC (2010) Chemotherapy resistance abrogation in metastatic melanoma. Clin Adv Hematol Oncol 8(4):259–266

Wang J, Chen X, Clarke ML, Chen Z (2006) Vibrational spectroscopic studies on fibrinogen adsorption at polystyrene/protein solution interfaces: hydrophobic side chain and secondary structure changes. J Phys Chem B 110(10):5017–5024

Yang Y, Sule-Suso J, Sockalingum GD, Kegelaer G, Manfait M, El Haj A (2005) Study of tumor cell invasion by microscopic Fourier transform infrared spectroscopy. Biopolymers 78(6):311–317

Zamble DB, Lippard SJ (1995) Trends Biochem Sci 20:435–439

Zwielly A, Gopas J, Brkic G, Mordechai S (2009) Discrimination between drug-resistant and non-resistant human melanoma cell lines by FTIR spectroscopy

Zwielly A, Mordechai S, Sinielnikov I, Salman A, Bogomolny E, Argov S (2010) Advanced statistical techniques applied to comprehensive FTIR spectra on human colonic tissues. Med Phys 37(3):1047–1055